Clays and Clay Minerals, Vol. 46, No. 3, 330–339, 1998.

ELECTRON MICROSCOPY AND X-RAY ANALYSIS OF LACUSTRINE CLAYS FROM THE CHARO CANYON, STATE OF MICHOACÁN, MEXICO

G. CARBAJAL DE LA TORRE,[1] I. ISRADE ALCÁNTARA,[1] J. SERRATO RODRÍGUEZ[1] AND J. REYES-GASGA[2]

[1] Instituto de Investigaciones Metalúrgicas U.M.S.N.H., Apdo. Postal 52 B, C.P. 58000 Morelia, Michoacán, México

[2] Instituto de Física, UNAM, Apdo. Postal 20-364, 01000 México, D.F., México

Abstract—In this paper we analyzed by electron microscopy and X-ray diffraction (XRD) the exposed lacustrine clay in a stratigraphic column at Charo Canyon, State of Michoacán, Mexico. Smectite, cristobalite, albite and quartz are the main mineral species in the sediments. Smectite is the most abundant and has a nanometric twinned small particle habit. The low crystallinity of the smectite detected in some of the samples seems to be associated with instability of the paleohydrological regime in which clayey material was deposited. Iron from underlying volcanic ash is apparently responsible for the iron concentration detected in the smectite structure.

Key Words—Clays, Electron Microscopy, Geology, X-Ray Analysis.

INTRODUCTION

The study of clayey materials is of great importance both for basic and applied research because of their ability to modify their structure in accordance with the surrounding environment and their many industrial applications, from ceramics, pillared interlayers and composites to catalysts, construction and water purification (Pinnavaia 1983; Sun-Kou 1992). They are phyllosilicates which, depending on their crystalline structure, include different types of clays such as illite, chlorinite, kaolinite, smectite and palygorskite (Brindley and Brown 1981; Linares 1983). The type of clay formed depends on the chemical and mineralogical composition of the parent rock and its weathering environment (Huang 1991). Weathering environments low in available moisture and high in Mg often form smectite; in regions where cations are more easily leached, kaolinite is favored; siliceous igneous rock precursors may form mica (illite), smectite or kaolinite. The plasticity of clays is a result of their small particle size, sheet-like structure and chemical properties, especially exchangeable cations and ability to sorb water (Kingery 1960; Brindley and Brown 1981). Their analysis and structural characterization is difficult because of variable water concentration, heterogeneity and high variability of structures and compositions. In the sedimentary basins of the Mexican Volcano Belt, clayey and silty diatomitic materials have been developed influenced by volcanic and tectonic activity along an east-west trending fault block, particularly in the state of Michoacán in the Cuitzeo paleolake. The study and characterization of the clays in this deposit and of the phenomena related to their formation are important for understanding the depositional mechanisms, and thus to analyze their potential application as catalytic materials. The purpose of this research is, therefore, the structural and chemical characterization of the clay minerals developed in the stratigraphic sediments of Charo, Michoacán, as a basis for understanding their sedimentary formation within the setting of the surrounding paleoenvironment and commenting on their possible application as catalytic materials.

GEOLOGICAL SETTING OF THE CHARO REGION

Charo is to the northeast of Morelia, the principal city of the State of Michoacán (Figure 1), at 1900 m above sea level. The Cuitzeo-Morelia region, as this zone is known, is controlled by a system of ENE-WSW oriented faults which cut the central sector of the Mexican Volcanic Belt. In particular, the lacustrine succession in the Cuitzel zone onlaps over a volcanic substrate which was dated 8 ± 0.2 million y (Albarran 1986). A volcanic cinder at the top of the lacustrine succession was dated 3.6 million y (Carranza-Castaneda 1976). Both the lacustrine and volcanic succession form a semi-graven 15 km long and up to 200 m deep. The Charo sector consists of Neogene fluviolacustrine deposits which crop out in the Charo Valley. Pliocene sedimentary facies mostly consist of unfossiliferous brown nonlaminated clays, alternating with sand, gravels, tuffs and diatomitic interbeds (Israde 1995). These sediments are not lithified. The stratigraphic range of lacustrine and fluviolacustrine sediments were deposited from approximately 3 to 8 Ma.

The samples analyzed in this research come from lacustrine strata which are composed of several layers of clay (Figure 1c), in the section "Las Pulgas". This section is in the center of the paleobasin located south of Charo Village. The outcrop was formed by fluvial erosion in which a succession of sediments of >40 m thickness can be observed. These strata can be related

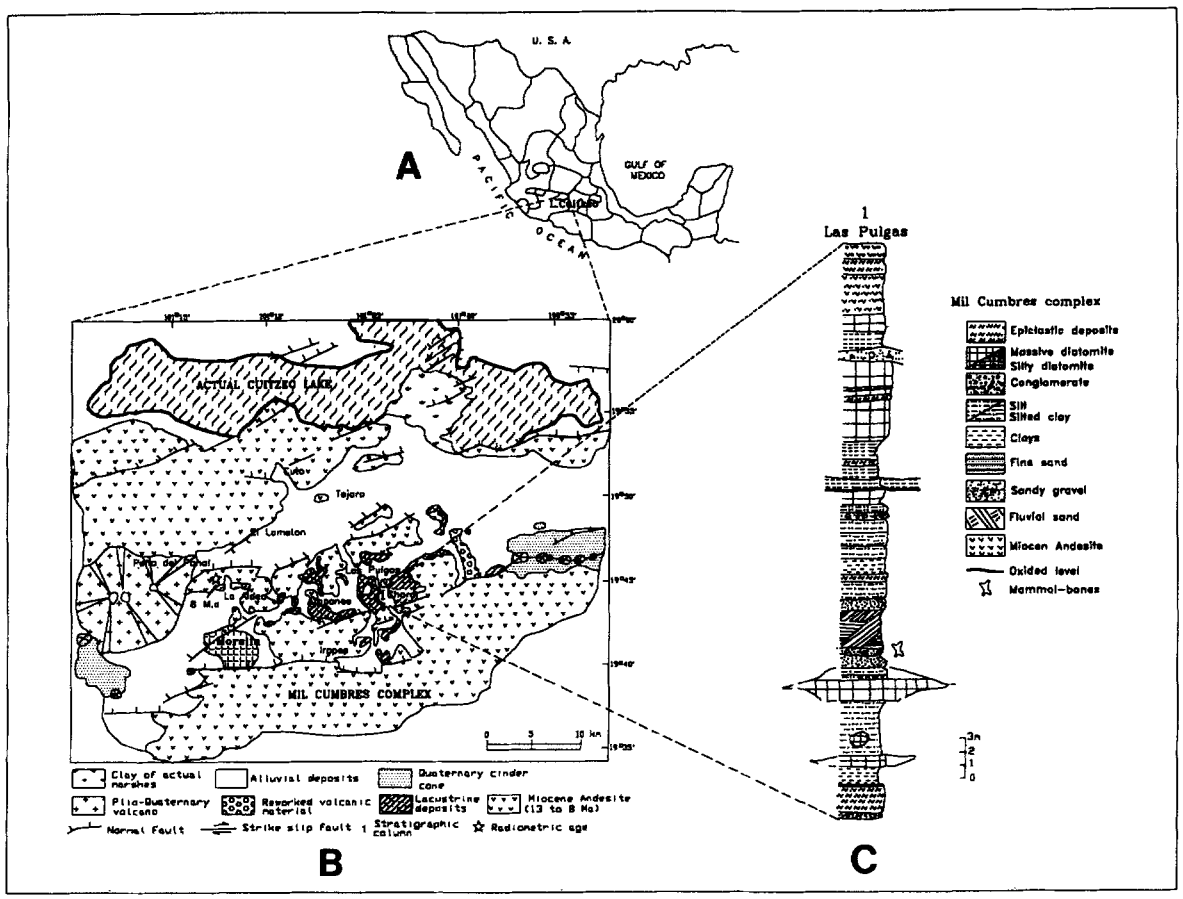

Figure 1. a) Schematic representation of Mexico showing the location of Cuitzeo basin, State of Michoacán, where the Charo Canyon is located. b) Geological Chart of the Morelia Cuitzeo zone. c) Layered section of the place named "Las Pulgas" where the samples were collected. The numbers indicate the layers from which the samples came (see text).

to climatic and/or tectonic events. The sedimentary succession is divided into 4 members:

1) Member A (levels 4 to 9 in Figure 1c): littoral facies composed of lacustrine sediments with silty, clayey and diatomaceous facies. This sedimentary deposit exhibits oxidized layers indicating fluctuations of water levels.

2) Member B (levels 9 to 16): deltaic, lacustrine and fluvial associations characteristic of sandy and interbedded silt facies commonly with macrophyte remnant and sporadic ash tuff levels. At the top is an areal exposure level indicative of a desiccation period.

3) Member C (levels 18 to 26): an open waterlike facies of diatomitic composition in which, at the top of the diatomite, there is an erosional discontinuity with the overlying sediments. A lake was developed at this time, and the open water facies were dominant. The lithology of this upper erosional member is dominated by clastic deposits, principally conglomerates and fluvial-deltaic sands, all of volcanic affinity.

4) Member D (levels 28 and 29): pyroclastic deposits have been found composed of millimeter-sized pumiceous material deposited generally in aqueous environments.

Some geological characteristics of the levels where clay was observed in the stratigraphic sequence shown in Figure 1c, from the bottom to top, are the following:

Level 4: A fine and massive sandy stratum whose base is a fine, clear-brown-colored clay, and which is overlaid with a strongly oxidized ocher-color layer. This level indicates a period of submersion.

Level 6: A black, very plastic and laminar clay stratum with a fine stratification and luster.

Level 8: An oxidized ocher-yellow silt with abundant clasts of diatomite.

Level 13: A fluvial-type package of thick sand with rounded grains. Remnants of organic materials from mammals, birds and macrophytes were found.

Levels 14 and 15: Clastic material composed of fine and homogeneous sand with volcanic matrix. This lev-

https://doi.org/10.1346/CCMN.1998.0460312 Published online by Cambridge University Press

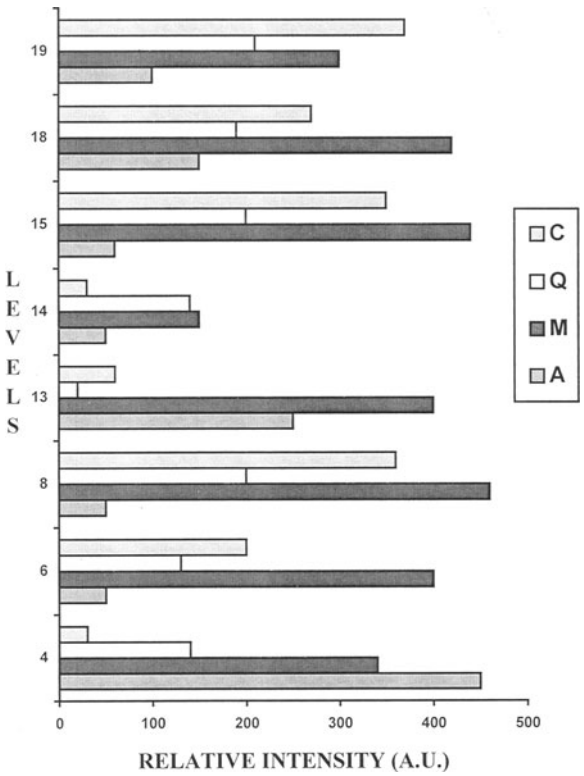

Figure 2. Semiquantitative clay concentration profile along the stratigraphical section shown in Figure 1c. The numbers along "Levels" axis correspond with those indicated in Figure 1c. Key: C = Cristobalite, M = Smectite, Q = Quartz, A = Albite.

el becomes more clayey at the top, where a fine sandy-silty horizon passes through a discordance of a paleosol with macrophytes that indicate low and well-oxygenated water.

Level 18: Silts and silty clays which are more compact at the top.

Level 19: Black plastic clay, laminae in 3-cm-uniform-thick layers.

EXPERIMENTAL PROCEDURE

After the geological study of the entire stratigraphic column (Israde 1995), the levels selected to analyze the clay type present were those indicated by numbers 4, 6, 8, 13, 14, 15, 18 and 19 in Figure 1c. Three kg of each sample were collected and stored in plastic bags. In the laboratory, a dried 500-g subsample of each was ground in an agate mortar and pestle to pass through a 325-mesh sieve. The resultant powder was further sieved to obtain material with a grain size less than 44 μm. This <44-μm powder still includes both clays (<2 μm) and silts (2–44 μm); however, unfortunately, we did not make any measurements of the silt/clay ratio. The product was stored in plastic bags in a desiccator.

Each sample was divided into 2 parts. One portion was washed with distilled water without the use of chemical reagents, dispersed in the ultrasonic cleaner for 7 h and dried at 110 °C for 24 h in an electric oven. The powder was analyzed by XRD. This heat treatment was done to compare the results with those reported in the literature (Brindley and Brown 1981). For XRD analysis, the powders were packed in a standard aluminum sample support with dimensions of 3 cm in diameter and 2 mm thick. The analysis was carried out using Cu$K\alpha$ radiation with a 2θ scan range from 2 to 65°. These data are summarized in the semiquantitative plot presented in Figure 2. The principal mineral species detected were cristobalite, smectite, quartz and albite. A second portion was kept for further processing in accordance with Zimmerman's procedure (Singer and Singer 1971).

As can be seen in Figure 2, in the middle of the column (between levels 13 and 14 in Figure 1c) there is a big diminution in the distribution of smectite, cristobalite and quartz while the quantity of albite increments. Therefore, taking in account this distribution along the column, the entire column can be divided into 3 regions and only 3 samples were selected for further structural analysis: those from levels 6 (S-1), 14 (S-2) and 18 (S-3). Figure 3 shows X-ray diffractograms of these <44-μm-grain samples from the 3 chosen layers of the Canyon; smectite shows the highest concentration. Comparing the shape of the peak set at 5° in the 3 diffractograms of Figure 3, there is an indication that the crystallinity of smectite is changed along the column. In Figure 3b this peak shows that amorphization has taken place in the middle level.

According to the Zimmerman method, liquid clay slurries were prepared by dispersion and gravitational sedimentation to separate the clays from silt fractions. The method consists of pouring 100 g of powder sample into a glass beaker together with 1 L of deionized water and putting the solution in the ultrasonic cleaner for 7 h. This allows the dissociation of silt grains and clays mixed together in the solution. Afterward, the solution is placed for sedimentation in a 2-L separation funnel within a container that allows maintenance of

→

Figure 3. X-ray diffractograms of the 4-mo-sedimented samples: a) S1 (the deepest stratum); b) S2 (the middle stratum); and c) S3 (the uppermost stratum). The smectite signal (M) appears in all the diffractograms but in the middle layer it is a little bit more amorphous than in the others (evidenced by the shape of the peak at 5°). C = cristobalite, Q = quartz and A = albite peaks.

https://doi.org/10.1346/CCMN.1998.0460312 Published online by Cambridge University Press

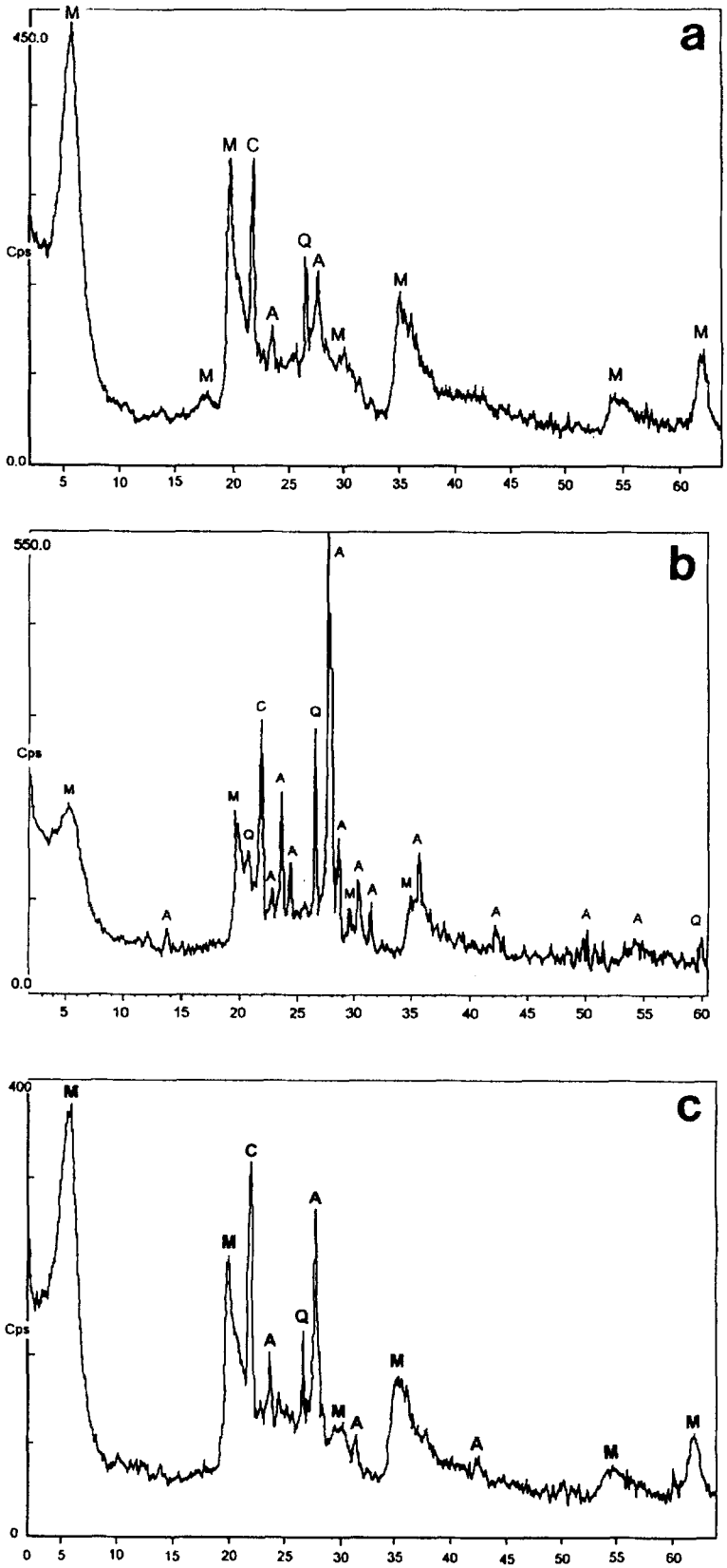

https://doi.org/10.1346/CCMN.1998.0460312 Published online by Cambridge University Press

Table 1. Chemical composition by X-ray fluorescence of the S1, S2, S3 samples (Figure 1c) from the clay of the Charo Canyon, State of Michoacán.

Element	Sample 1 wt%	Sample 2 wt%	Sample 3 wt%
Mg	0.32	0.33	0.37
Al	9.22	9.47	10.22
Si	28.63	28.53	31.65
P	0.74	0.07	0.07
K	0.64	0.57	0.79
Ca	0.60	0.82	0.90
Ti	0.54	0.45	0.47
Fe	3.43	5.90	5.05
O	44.18	44.51	48.48
Total	88.31	90.65	98.00

a constant temperature (22 °C) during settling to prevent convection currents from mixing the sample. The sedimentation time, following the method, must be 3 to 4 mo, until the sedimenting solution color becomes whitish. This procedure guarantees that the clayed material will be the last deposited with particle size of approximately 100 nm. For further analysis, material was collected from the last layer sedimented after 4 mo for each of the 3 selected levels. These samples were stored in small plastic bottles.

For transmission electron microscopy (TEM) observation, a small quantity of the collected material was suspended in deionized water and a drop was placed on a copper grid previously coated with a thin carbon film, and dried. For scanning electron microscopy (SEM), pieces of sedimented material were dried and coated with Au or Cu thin film.

Electron microscopy analyses were carried out both in a JEOL 6400 SEM, which has NORAN energy dispersive spectral (EDS) equipment attached, and a JEOL 100-CX analytical TEM, with KEVEX-EDS equipment. The X-ray diffractograms were obtained using a SIEMENS D-5000 diffractometer and the X-ray fluorescence (XRF) analysis in a KEVEX 4000 microanalyzer.

RESULTS

The top of the 4-mo-sedimented material was analyzed by XRF to discern their main chemical components. These results are shown in Table 1. The principal elements found in these samples were, from high to low amounts, Si, Al, Fe, O, P, Ti, Ca, K and Mg. From these elements, those which show more variation in their concentration among the 3 samples are P, Fe, Ca and K. Phosphorus concentration exhibits an increase from the basal strata toward the upper one in 1 order of magnitude, indicating an organic matter enrichment. It is also evident that Ca and Si concentration increase with the upper layers.

SEM images from the samples show the typical morphology following the sedimentation process (Figure 4). These samples are formed by aggregates of nano-sized particles which, with the best resolution obtained, seem to be in the order of 100 nm. The general EDS X-ray microanalysis from these samples (Figure 5a) shows the elements O, Al and Si (the Cu signals come from the Cu film which covers the sample for its SEM observation). However when the X-ray spectrum is taken from the well-defined crystallites, such as the one shown in Figure 4c, the spectrum shows C, Ca, Fe and Mg besides the mentioned elements (Figure 5b). In Figure 5c the EDS spectrum from a synthetic Ca-montmorillonite is shown just for comparison with those shown in Figures 5a and 5b. In this case, the main elements are O, Al, Si and Mg (the synthetic clay was covered with a carbon thin film, producing the C peak). The C peak in spectra shown in Figures 5a and 5b was produced from some remnant of organic material. In Figure 5b, an Fe peak is identified. TEM analysis gives additional information on the structure of the clay minerals. In the case of smectite, the TEM images always show small particles of nanometric size (Figure 6) whose grains were always observed thick in their center (more than 200 nm) and with smoothed edges. In bright field images the particles' contrast appears dark (Figure 6a), but in dark field images this contrast is good enough for observing thickness fringes (Figures 6c and 6d), giving an idea of their shape (Heinemann et al. 1979). The other clay minerals presented their common TEM contrast (Oberlin 1961).

The smectite particles were always observed formed by 2 smaller grains whose structural relationship among them is twinning (Figure 6b). The effect of twinning on the electron diffraction (ED) patterns gives more spots and produces more confusing patterns than in the untwinned case. Of course, the observation of twinned reflections depends on the orientation of the grain with the electron beam direction and the thickness of the twin boundary. However the twinned reflection indexation is easily solved. Figure 6b shows that the reflection arrangement in this diffraction pattern follows the superposition of 2 identical parallelogram figures related by a rotation of 180° relative to each other. Figure 7 shows another 2 ED patterns of the smectite particles but along untwinned axes. Their indexation indicates a pseudohexagonal unit cell with parameters a = 0.51, b = 0.90 and c = 1.8. nm corresponding to the montmorillonite clay (MacEwan 1944; Earley et al. 1953).

DISCUSSION

We have used different techniques to get the benefits of multiple analytical combinations and to produce a more complete characterization of the samples. Among these analytical techniques we would like to highlight the use of TEM coupled with EDS X-ray instruments, as the structural and chemical analyses at

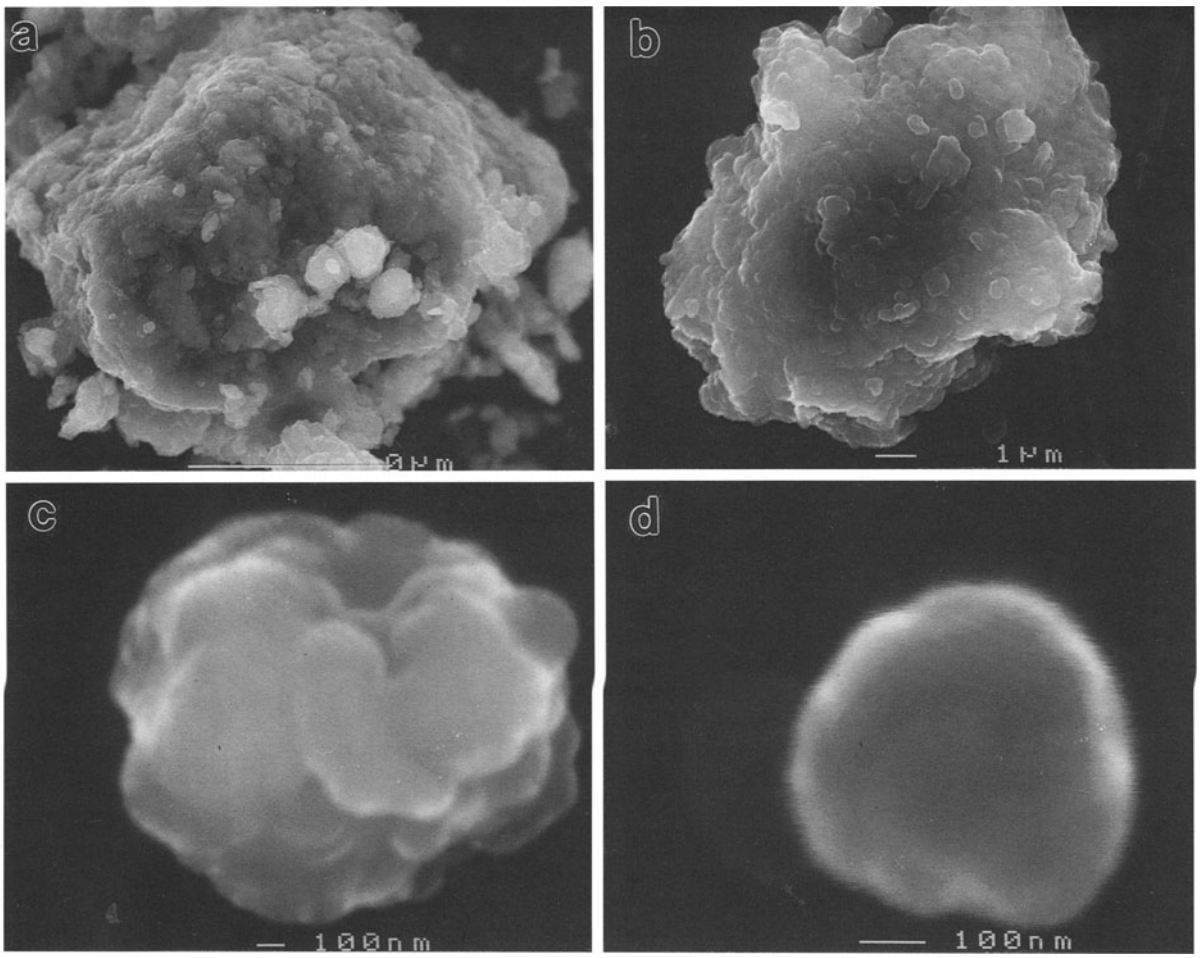

Figure 4. SEM images of the smectite clay at different magnifications. Note that grain in (a) is formed by a conglomeration of nanometric particles like the one shown in (d).

different levels of resolution are much easier. In the clayey material field, this information is invaluable. For example, in TEM the smectite was observed as nanometric small particles formed by 2 grains that are related by twinning—structural information which has to be taken into account in future work on modeling.

The distributive province to which the Charo Canyon belongs has been derived through mechanical erosion and exposed to intense chemical weathering. During a subsequent humid phase, the volcanic material could be diagenetically transformed to clay in a confined calm water environment. Particularly the abundance of Al, Fe and P are of great interest in the study of this region, because they give some clues on its geological evolution. The concentration of phosphorous oxide in the basal sector was most likely produced by the abundant animal and vegetal activity together with high production of overlying diatoms characteristic of swampy environments. The Fe enrichment is derived from the underlying volcanic ash, which also indicates an increment in the volcanism of this region. The high abundance of Al in level 18 corresponds to the epiclastic sediments underlying this level. Moreover, the absence of Na in the sediments indicates that the Paleo-Cuitzeo lake was nonsaline without an important evaporation regime.

XRD showed that all of the analyzed samples contained the same smectite (possibly montmorillonite type) along the lacustrine succession; the main difference observed was the degree of crystallinity. From the diffractograms of Figure 3 and taking into account the shape of the peak at 5°, it is deduced that smectite in the middle of the column is much more poorly crystalline than that in the top and bottom layers. The amorphization or not-well-developed structure of the smectite could be produced by the way the material was deposited in this package, in which clays were alternated with silts, sands and tuffs in an aqueous environment. In the middle of the column these materials fell into turbid water in such a way that a clay

https://doi.org/10.1346/CCMN.1998.0460312 Published online by Cambridge University Press

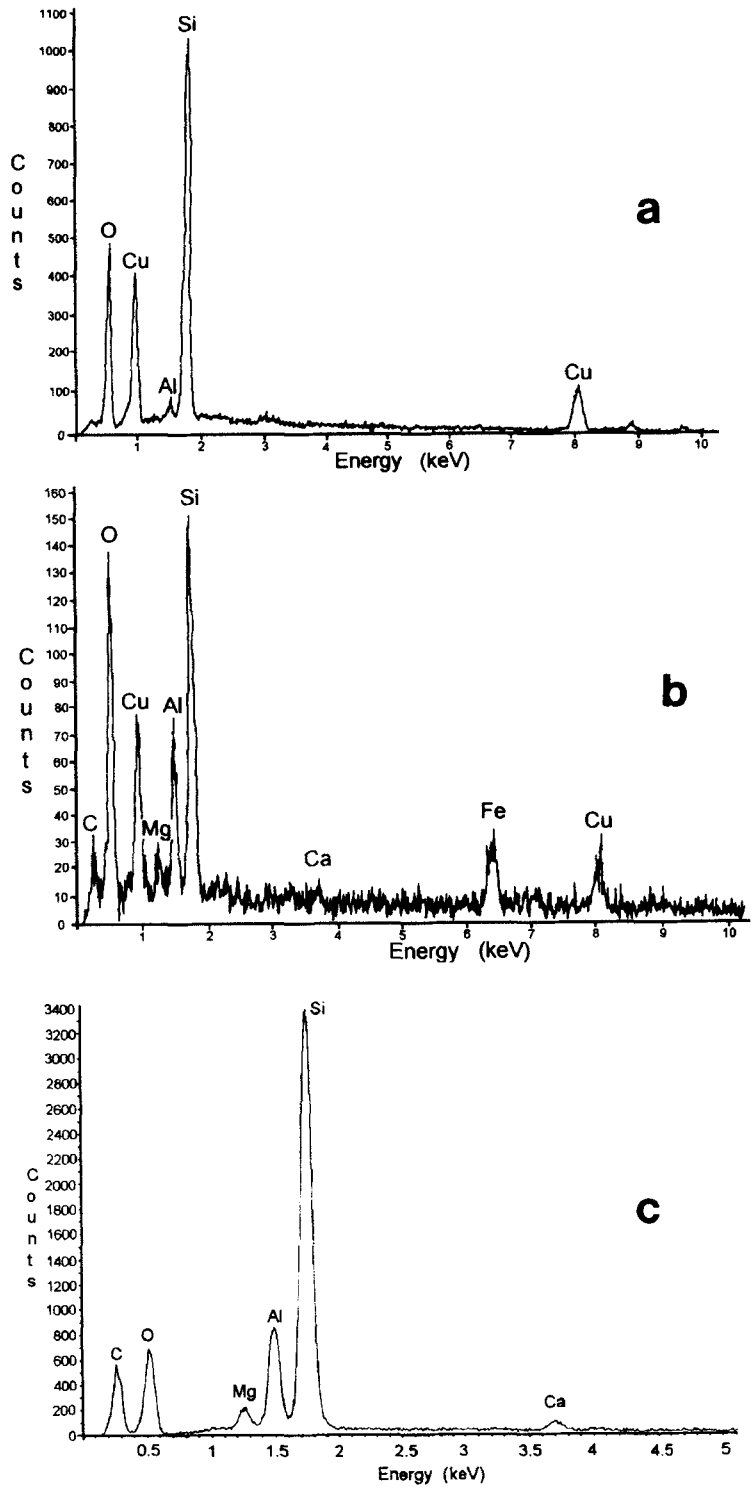

Figure 5. EDS X-ray spectra. a) General spectrum; b) spectrum from the particle shown in Figure 4d; c) spectrum from synthetic Ca-montmorillonite. In (a) and (b) the Cu peak comes from the thin film which covers the samples, whereas in (c) the sample was covered with a carbon thin film for SEM observation. Note in (b) the appearance of a Fe peak but not in (c).

https://doi.org/10.1346/CCMN.1998.0460312 Published online by Cambridge University Press

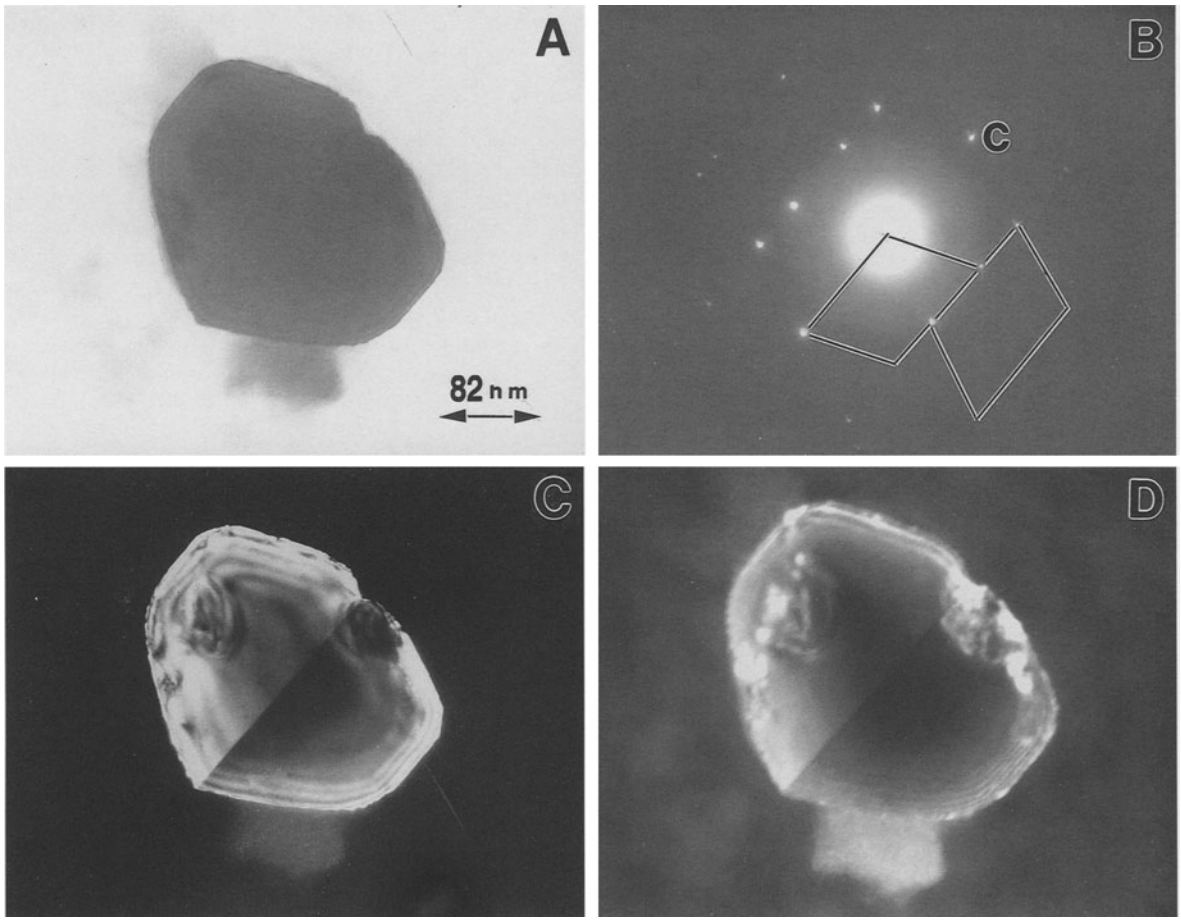

Figure 6. TEM images of one of the smectite grains. a) Bright field image; b) diffraction pattern showing the spot splitting produced by twinning; c) Dark field obtained with the spot indicated with "c" in (b), d) Dark field obtained with the "c" spot but in weak beam conditions.

deposition was inhibited, producing the diminution in the distribution observed in Figure 2. In the other levels of the column there was a greater deposition of these clays because a more calmed sedimentation was possible. Cristobalite is derived from volcanic origin caused probably by lithostatic pressure.

From the structural point of view, however, it was not possible to find any structural change, at least with the electron microscope resolution, among the crystalline smectite grains coming from the 3 different depths chosen. This was true although the number of particles whose ED patterns show 2 diffuse concentric halos, a characteristic of amorphous structures, was bigger in samples from the middle depth. For a better quantification of the amorphous material, the electron microscope sample preparation technique must be improved and used together with another technique to obtain more information on the structural differences. This additional technique could be scanning probe microscopy (SPM).

The studied region is located in the sedimentary basins of the Mexican Volcano Belt, that is, in an Fe-rich depositional environment. Therefore, the Fe detected in the clayey minerals is a result of the volcanic ash deposited in this region. For many years clays and this ash have been together such that Fe has been diffused into the clay structures, quite expectable with the many free pathways existing in these minerals. Thus, the lacustrine clays from the Charo Canyon present some proportion of Fe-enrichment.

Clays are used in catalysis because their catalytic activity on organic molecules is higher than that of zeolites. This behavior is a result of their more open channels, which allow a better diffusion of organic molecules and water. The intercalation of inorganic atoms such as Al, Ti or Zr in the interlayed space produces an expansion along the *c*-axis up to 1.9 nm. Moreover, there is a negative charge distribution by the substitution of some cations, such as Al^{3+} for Mg^{2+} and Fe^{2+} and Si^{4+} for Al^{3+}, which is compensated by

https://doi.org/10.1346/CCMN.1998.0460312 Published online by Cambridge University Press

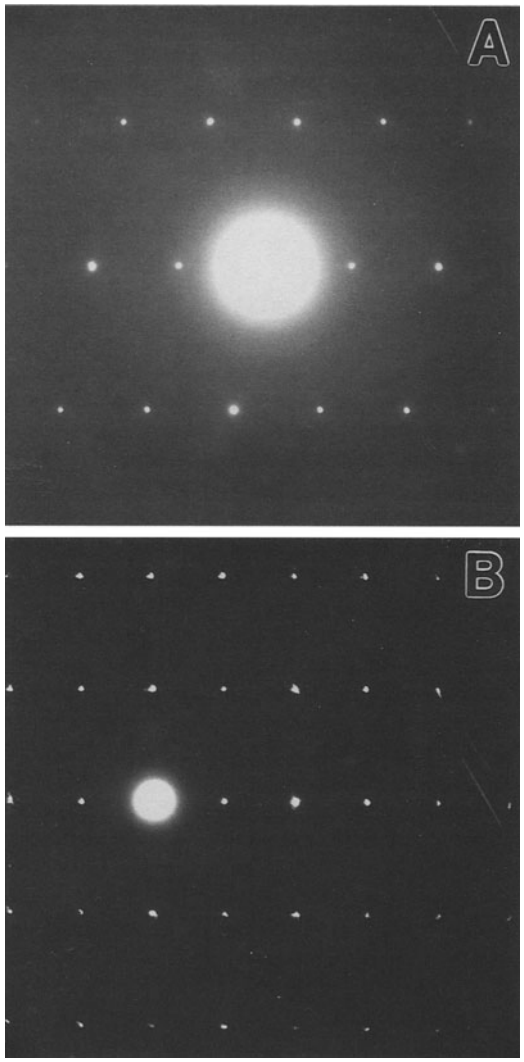

Figure 7. Selected AED patterns from smectite grains along untwinned axes zone.

cations such as Na^+, K^+ and Ca^{2+}. This possibility of inserting foreign cations into the clay structure is the basis of a new branch of molecular engineering whose objective is the tailoring of new catalytic materials with better properties. The properties more interesting in this area are the hydrothermic stabilization, the superficial acidity (responsible for the catalytic activity) and the microstructure of the clays.

Montmorillonite is used in catalysis as catalytic support when it is doped with Al and Zr (Sun-Kou et al. 1992). The clays mentioned in this work have not been analyzed for their catalytic capabilities, but the smectite, which seems to be of the montmorillonite type, can be processed to render a clay which may eventually be used for catalytic applications. The presence of Fe in the smectite structure favors its catalytic properties because Fe stabilizes the structure to increment the absorption of organic molecules through their interlayer space. It is necessary to determine if this volcanic ash Fe is appropriate for the catalytic use of smectite, because a natural Fe insertion could present different properties than a synthetic Fe enrichment. Moreover, the materials mined for catalytic applications are generally quite pure and should not need to be purified because of the high cost of purification (Earley et al. 1953). The materials analyzed here present minerals that could hinder their catalytic potential. The influence of, for instance, Fe in the structure of these materials must be analyzed before any catalytic consideration. That is the future beyond this study.

CONCLUSIONS

Smectite, cristobalite, albite and quartz are the main mineral species in the lacustrine region of the Charo Canyon. Twinning, the unique crystalline feature not reported for smectite elsewhere, is associated with the nanometric clay grains. From the chemical and structural study of the stratigraphic column it can be concluded that the major depositional sediments were produced when there were calm sedimentary depositional environments whose clays had better crystalline structures; however, the clay minerals are found in an environment rich in Fe because of the underlying volcanic ash common in this region. The advantage (in catalysis) of the insertion of Fe atoms in the clay structure is known but, before making any assertion on the catalytic use of smectite clay from the Charo Canyon, further analyses must be made on the influence of Fe in its structural properties. Also, a financial analysis of the purification process must be performed to show its viability.

ACKNOWLEDGMENTS

We acknowledge the fruitful discussions about this work with A. Cordero. A. Negron, S. Ramos and Agostino Rizzo. We want also to acknowledge the technical help of F. Solorio, T. Alfaro, P. Mexia, L. Rendón, M. A. Epinosa Medina, E. Hernández, C. Zorrilla, S. Tehuacanero and R. Hernández. This work has been supported by DGAPA-UNAM (through project IN-106295) and CONACYT-SIMORELOS (through project 9506063).

REFERENCES

Brindley GW, Brown G. 1981. Crystal structures of clay minerals and their X-ray identification. London. p 157.

Carranza-Castaneda O. 1976. Rhynchotherium falconeri del rancho La Goleta, Michoacán, Mexico. Proc Congreso Latinoamericano de Geología 3. p 28.

Earley JW, Osthaus BB, Milne IH. 1953. Purification and properties of montmorillonite. Am Mineral 38:707–710.

Heinemann K, Yacamán MJ, Yang CY, Poppa H. 1979. The structure of small, vapor-deposited particles. J Cryst Growth 47:177.

Huang WT. 1991. Petrologia, Limusa Editor. México. p 301–320.

Israde I. 1995. Bacini lacustri del settore centrale dell'Arco Vulcanico Mexicano. Stratigrafia ed evoluzione sedimentaria basata sulle diatomee. [Ph. D. thesis]. p 254–256.

Kingery WD. 1960. Ceramic fabrication processes. Technology Press, M.I.T. and J. Wiley, New York. 420 p.

Linares J. 1983. La arcilla como material cerámico, características y comportamiento. Cuadernos de Prehistoria de la Universidad de Granada, No. 8. Granada, España. 60 p.

MacEwan DMC. 1944. Identification of Montmorillonite. Nature 154:577–579.

Oberlin A. 1961. Etudes morphologiques et structurales. In: Traité de microscopie électronique, vol. I, C. Magnan Edition Scientifiques Hermann. p 525–551.

Pinnavaia TJ. 1983. Intercalated clay catalysts. Science 220: 365–366.

Singer F, Singer SS. 1971. Ceramica Industrial. In: Enciclopedia de la Química Industrial, vol. I, No. 9, Ediciones Urmo, España. p 74–87, 286–294, 347–367.

Sun-Kou MR. 1992. Caracterozación de una montmorillonita española con pilares Al y Zr. In: Boletín de la Sociedad Española de Cerámica y Vidrio. 31–4:293–397.

(Received 18 November 1996, accepted 3 November 1997; Ms. 2747)